Cavitation in liquid metals under negative pressures. Molecular dynamics modeling and simulation

2008 J. Phys.: Condens. Matter 20 114113

(http://iopscience.iop.org/0953-8984/20/11/114113)

IOP PUBLISHING JOURNAL OF PHYSICS: CONDENSED MATTER

J. Phys.: Condens. Matter **20** (2008) 114113 (11pp) doi:10.1088/0953-8984/20/11/114113

Cavitation in liquid metals under negative pressures. Molecular dynamics modeling and simulation

T T Bazhirov, G E Norman and V V Stegailov

Joint Institute for High Temperatures of Russian Academy of Sciences, Izhorskaya street 13/19, 125412 Moscow, Russia
and
Moscow Institute of Physics and Technology (State University), Institutskii pereulok 9, 141700 Dolgoprudny, Moscow Region, Russia

E-mail: bazhirov@ihed.ras.ru, norman@ihed.ras.ru and stegailov@ihed.ras.ru

Received 12 November 2007, in final form 31 December 2007
Published 20 February 2008
Online at stacks.iop.org/JPhysCM/20/114113

Abstract

An approach to study cavitation in stretched liquids via molecular dynamics (MD) simulation is presented. It is based on the stochastic properties of MD and allows one to study cavitation as a stochastic phenomenon. The approach is used to study equation of state and stability limits of the metastable liquid phase, cavitation kinetics and dynamics properties for different temperatures. Particular examples of metals under consideration include Pb, Li and $Pb_{83}Li_{17}$. Quantitative and qualitative disagreements between the classic nucleation theory estimates and the MD results are found. The Kolmogorov–Johnson–Mehl–Avrami equation is used as an alternative way to estimate cavitation rate. The two methods show good mutual agreement. Decay at a constant stretching rate is also considered.

1. Introduction

The cavitation process consists of two main stages: bubble formation and its subsequent collapse inside the metastable liquid. The metastable liquid phase can exist as a stretched or/and a superheated state. Both cases are equal from the thermodynamic point of view. The traditional method for describing the kinetics of cavitation is the classic nucleation theory. It is based on thermodynamic calculations of the work of new phase nucleus formation and on the solution of the kinetic equation for the size distribution of nuclei [1–7]. The use of classic nucleation theory in practice, especially at negative pressures, is often complicated. It happens due to the uncertainty in the actual accuracy of model concepts taken into consideration and the absence of both reliable data on the surface tension at the interphase boundary and the equation of state of metastable liquids. The use of the classic nucleation theory is also limited by the closeness of the thermodynamic state to the phase stability limits (spinodal) [3–7].

Using the molecular dynamics (MD) method allows one to study cavitation on the microscopic level, based only on interatomic interaction potentials without additional assumptions on the mechanisms of cavity formation and growth. For instance, the appearance and growth of a localized vapor nucleus was clearly seen and the kinetic stability limit of liquid was estimated in a system of 10 976 particles in [8]. A method for calculating the frequency of homogeneous nucleation in a metastable phase simulated by the MD method was suggested in [9–11] for the nucleation in a superheated crystal. This method was based on averaging the metastable phase lifetime over an ensemble of independent molecular dynamics trajectories. A similar approach was used to calculate the cavitation rate in a Lennard-Jones liquid in [12, 13], where the influence of the cutoff radius of interparticle interaction potentials was analyzed. The cavitation dynamics and kinetics for an embedded-atom model (EAM) of liquid lead under negative pressures in a wide range of temperatures were studied in [14–16]. In [17] the Lennard-Jones MD model was used to investigate a collapse process of a single gas bubble in the liquid—the second stage of cavitation, which is an elementary process relevant to sonoluminescence. As the bubble shrinks after a uniform compression of the system, a sharp temperature rise and a significant heat and mass transfer on the surface were observed.

Cavitation has a very harmful effect. For example, when a propeller blade is rotating through the water the

latter becomes stretched and cavities grow; this is the most common implementation of a cavitation process; when voids collapse the resulting pulses can cause propeller material destruction. There are many of examples of this kind. Though there are some cases in which cavitation is useful and desirable [18, 19], it would be a great achievement to avoid cavity formation in most areas of industry. The same kind of undesirable processes could possibly influence the work of a new type of energetic reactors with fast deuterium–tritium fuel ignition (FIHIF—fast ignition heavy ion fusion) [20–22]. The performance of systems of this type is substantially influenced by continuity loss (cavitation) in the coolants caused by the relaxation of stresses that arise as a result of micro-explosions in the working chamber (e.g. see [23, 24]). In order to simulate system functioning, we have to use the data on the kinetics of cavitation in the heat-transfer material under tensile stresses [25]. Liquid Pb, Li and $Pb_{83}Li_{17}$ were selected as the objects of study because they are the basic components of promising coolants in FIHIF reactors.

In this work we are presenting an approach to study cavitation in stretched liquid via MD simulation. It is shown that cavitation is a stochastic phenomenon, so the lifetime of a stretched liquid is a random value and the decay of the liquid is a Poisson process. The approach presented consists of three main stages: (a) modeling of the ensemble of initial states which are different from each other microscopically but equivalent to each other from the macroscopic point of view; (b) simulation of the ensemble of MD runs in order to study spontaneous decay, to obtain an equation of state with spinodal included, lifetime distribution, average lifetime and cavitation rate J; (c) analysis of pressure and temperature dependence of J, elucidation of stability criteria and comparison with different variants of classic nucleation theory. Examples are given for the melts of lead, lithium and $Pb_{83}Li_{17}$ using the EAM potentials. Various MD diagnostics are applied. Qualitative and quantitative disagreements with the classic theory of homogeneous nucleation are found. The cases of cavitation at both static negative pressures and stationary stretching rates are treated.

2. MD method theory and model used

2.1. Model and method of calculations

Interatomic interactions are described by a many-particle potential for Pb, Li from the set of EAM type potentials [26, 27] suggested in [28, 29]. These potentials fit better for modeling metals than common pair potentials (Lennard-Jones type, for example) since they explicitly take into account the effective electron density function. Addition of the many-body effects to the classical pair potential brings the computed material properties (such as temperature dependence of free energy, melting point, thermal expansion coefficients, Gruneisen parameters, elastic constants and defect properties) to within the range of their experimental values for many metals [30]. It is well known that the vacancy formation energy calculated from a pair potential is significantly higher than those obtained from experiment even for a rare-gas solid. Addition of the many-body interactions reduces this energy to be more in agreement with experimental values. This fact is especially important for the case of cavitation at the initial stage of bubble formation since the bubble initially is formed as a 'vacancy' in liquid. The work of the critical bubble formation is the most important factor determining all the kinetic properties of cavitation. Because of the inclusion of the many-particle contribution, it can be expected that the EAM potentials describe the behavior of particles on an open surface, and therefore all phenomena related to liquid–gas phase transitions, better than pair potentials. Thus, we can see the importance of introducing many-body interactions. Potential energy in our model can be represented by the sum of two terms:

$$U = \sum_{i<j} \phi(r_{ij}) + \sum_{i} F(\bar{\rho}_i). \tag{1}$$

The first term corresponds to pair interactions: ϕ is the pair interaction potential. The second term describes many-particle interactions; the embedding function F in it depends on the effective electron density on atoms ρ. The latter is in turn a function of the distance r_{ij} between i and j atoms:

$$\bar{\rho}_i = \sum_{j \neq i} \rho(r_{ij}). \tag{2}$$

The effective electron density in this form properly describes the electronic interaction induced part of the potential energy for the spherically symmetric electronic configuration possessing atom types. It happens because this function depends only on the interatomic distance. Thus, the total potential energy of the particular atom is a sum over the neighbor list (the atoms within a cutoff sphere; the cutoff radii values are taken from the original articles [28, 29]) of pair interaction energies between atoms plus the value of a function F applied to effective electron density on the atom. It is also induced by all the atoms within the same cutoff sphere and it is calculated by a summation over the neighbor list.

The lead potential parameters were adjusted in [28] using the condition of correspondence to the properties of the crystalline phase (its binding energy, surface energy, elastic constants, phonon frequencies, thermal expansion, and temperature of fusion). This potential was successfully used to study surface and cluster fusion and crystallization and vaporization of nanoclusters [31]. It was, for instance, shown that the temperatures of fusion (618 ± 4 K) and vaporization ($\sim$2050 K) of molecular dynamics models based on this potential were in close agreement with the experimental values for lead (600.7 and 2033 K, respectively). In [29], the authors have constructed the potential for Li from first-principles calculations. The potential was shown to be very good at describing the structural properties of bulk metals and clusters in the size range $8 < N < 310$. The lattice constant, melting temperature, vibration modes, bulk modulus, and Gruneisen constant are in agreement with available experimental values.

The molecular dynamics method consists of numerical integration of the equations of motion of the many-particle system according to the previously specified interaction potential between them. The equations of motion in our case

represent the classical Newtonian equations:

$$m_i \frac{\mathrm{d}\vec{V}_i(t)}{\mathrm{d}t} = \vec{F}_i[r(t)] \qquad \vec{V}_i(t) = \frac{\mathrm{d}\vec{r}_i(t)}{\mathrm{d}t}$$
$$\vec{F}_i[r(t)] = \frac{\partial U}{\partial \vec{r}_i} \tag{3}$$

where r_i is the ith particle vector coordinate and U is the potential energy of the system. Constant temperatures were set and maintained using the thermal stabilization scheme (thermostat). Additional Langevin terms were introduced into the equations of motion, namely, self-consistent white noise and friction [32, 33], whose total influence was small compared with that of interatomic interaction forces.

In this work, we consider systems with 13 500–500 000 atoms in the basic cube. Three-dimensional periodic boundary conditions are used. The trajectories of atomic motions are calculated by the numerical integration of the system of classical equations of motion using the difference scheme of the second order of accuracy with a 1.43 fs time step. The instantaneous temperature (T) and pressure (P) averaged over the cell volume are calculated as

$$T = \frac{2m}{3k_\mathrm{B}N}\sum_{i=1}^{N}\frac{v_i^2}{2}, \qquad P = \frac{1}{V}\left(Nk_\mathrm{B}T + \frac{1}{2}\sum_i \vec{F}_i\vec{r}_i\right), \tag{4}$$

where k_B is the Boltzmann constant, m is the mass of the atom, V is the calculation cell volume, and $\boldsymbol{F}_i$ is the force acting on particle i.

2.2. Stochastic properties of EAM model

The dynamic system of many particles possesses stochastic properties [34, 35]. It can be revealed as a cause of exponential divergence of MD calculation trajectories. In the course of time, the system under consideration could no longer be described by the analytical solution of the initial system of equations of motion (e.g., if we calculate a trajectory using both analytical solution and the MD finite-difference approach, we will see an exponential divergence). In this case we have to use the concepts of dynamical memory time and Krylov–Kolmogorov entropy. Here it is necessary to emphasize that an exponential trajectory divergence is a feature of the many-particle system itself (N-equation Cauchy problem feature), not only of the MD model. In MD calculations numerical errors just initiate the divergence process.

The dynamical memory time can be specified from the following procedure. First it is necessary to calculate the coordinate or the velocity divergences:

$$\langle \Delta r(t)^2\rangle = \frac{1}{N}\sum_{i=1\ldots N}\left(r_i(t) - r_i'(t)\right)^2$$
$$\langle \Delta \upsilon(t)^2\rangle = \frac{1}{N}\sum_{i=1\ldots N}\left(\upsilon_i(t) - \upsilon_i'(t)\right)^2 \tag{5}$$

where (υ, r) and (υ', r') are the coordinate and the velocity on the first and on the second trajectory, respectively. For the numerical solutions of the N-equation Cauchy problem we have then

$$\langle \Delta r(t)^2\rangle = A\exp(Kt) \qquad \langle \Delta \upsilon(t)^2\rangle = B\exp(Kt) \tag{6}$$

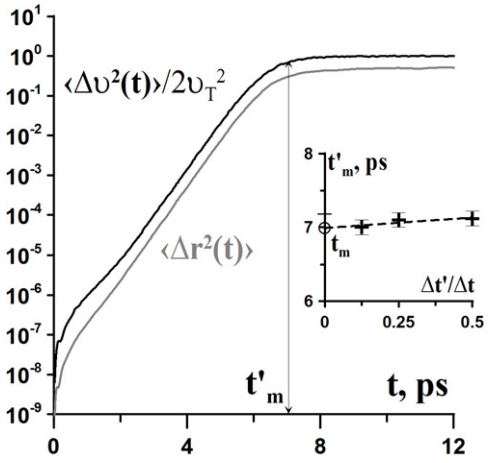

Figure 1. The coordinate (lower) and the velocity (upper) divergence time evolution in MD calculation for the values of timesteps $\Delta t = 0.005$ and $\Delta t' = 0.0025$ ps. It is seen that the correlation is lost at approximately 7 ps when the system meets the condition $\langle \Delta \upsilon^2\rangle = 2\langle \upsilon^2\rangle_T$. In the inset there is a dependence of time of divergence on the timestep ratio (timesteps used: $\Delta t = 0.005$; $\Delta t' = 0.0025, 0.001\,25, 0.000\,625$ ps).

where A and B are the constants that depend on the initial perturbation values and K is the maximum averaged Lyapunov entropy. As a consequence of the above described instability, MD trajectories calculated from the same initial configuration with different integration timesteps Δt and $\Delta t'$ diverge exponentially fast (see figure 1). The finite difference character of integration results in the fact that resulting trajectories do not coincide right after the first timestep of calculation. In a certain period of time the divergence changes its exponential character and goes to saturation at t'_m. After this moment two trajectories are completely uncorrelated as if their initial configurations were not the same. The limiting value $t_\mathrm{m} = \lim_{\substack{\Delta t\to 0\\ \Delta t'-\mathrm{fixed}}} t'_\mathrm{m}$ is called dynamical memory time. In the EAM model used in this work the value of dynamical memory time is estimated and is approximately equal to 7 ps (see figure 1). Such a small value of dynamical memory time means that one could obtain two statistically completely independent trajectories from one initial condition using two different integration steps after about 7 ps of calculation.

The given property of molecular-dynamical systems allows us to apply MD to modeling processes of formation of a new phase in view of metastability. When the average lifetime of a metastable phase is greater than the dynamical memory time, the lifetime distribution is subject to Poisson statistics as the calculations show.

3. Homogeneous nucleation

3.1. Simulation of the ensemble of the MD runs

Instead of the above described method of obtaining statistically independent configurations, in this work we use another approach to generate the initial states (see [10] for some discussion). The initial configuration of atoms corresponding to the liquid phase is generated as follows. First, a

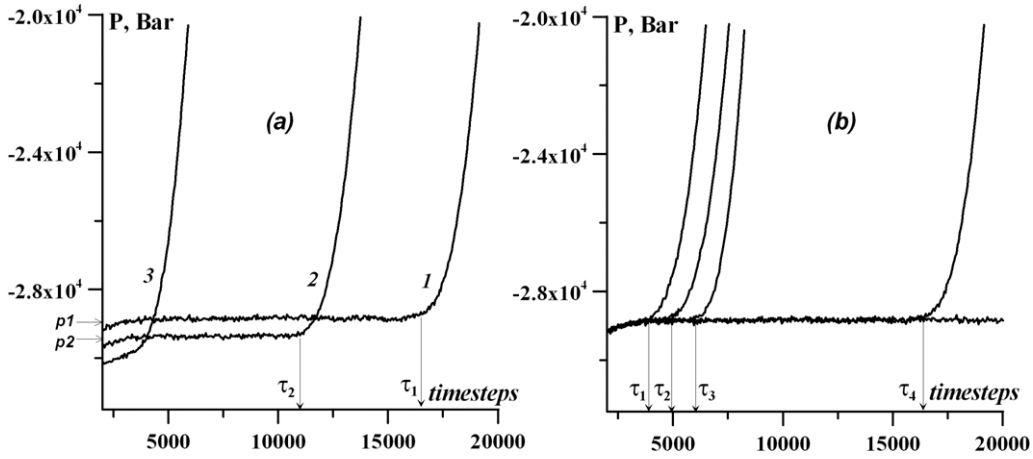

Figure 2. Typical pressure on time dependences in MD calculations (timestep = 5 fs). (a) Macroscopically different initial states 1 and 2 produce systems with different pressures inside, P_1 and P_2, and different lifetimes, τ_1 and τ_2. Case 3 in which the system does not have any distinguishable value of lifetime is also shown. (b) Microscopically different initial states (having different implementations of Maxwellian atomic velocity distribution for the same temperature) have different values of lifetime τ_1–τ_4 for the same value of pressure.

configuration which is a face centered cubic (FCC) lattice of atoms with the required density $\rho = mN/V$ and velocities randomly selected according to the Maxwell distribution corresponding to temperature T is constructed. Liquid metastable states at density and temperature values that excluded the possibility of solid phase existence are studied. For this reason, the lattice then undergoes fusion in several dozen femtoseconds during molecular dynamics trajectory calculations, and the system becomes a liquid with the given temperature T, which is then maintained by the thermostat for several picoseconds. The final configuration of preliminary molecular dynamics calculations is the sought initial configuration. We use different implementations of initial Maxwellian velocity distributions corresponding to the same temperature and density to produce an ensemble of independent initial configurations corresponding to the liquid at the given ρ and T.

In figure 2 the particular dependences of pressure on time in an MD simulation of cavitation in stretched liquids are shown. The horizontal part corresponds to the metastable liquid state. Then the pressure jumps upward and this moment corresponds to the cavity formation. There are two values we obtain from this calculation: the value of pressure inside the metastable stretched liquid and the value of its lifetime. If we start varying the volume of the system (or the level of stretching in other words), we will see that the corresponding pressure in it and its lifetime are also changing. The way in which pressure is changing specifies the equation of state. By averaging the value of lifetime over the ensemble of initial configurations it is possible to calculate kinetic properties of cavitation. Both these cases are described below.

3.2. Equation of state at negative pressures

We considered cavitation in the liquid at large negative pressures corresponding to states close to the stability limits (spinodal). Experimental data on liquid metal spinodal under negative pressures (including Pb and Li) are currently unavailable. General liquid phase diagram characteristics in the region of negative pressures at low temperatures ($0 < T < 0.5T_C$) have also been poorly studied (e.g., see [36]).

Equation of state calculations for the molecular dynamics model under consideration are performed by calculating the P–ρ dependence along isotherms and determining the $(\mathrm{d}P/\mathrm{d}\rho)_T = 0$ point by extrapolation (see figures 3(b) and 4(b)). Molecular dynamics trajectories 50–200 ps long are calculated for all densities studied at a fixed temperature. The average lifetime of metastable liquids τ decreases as the density lowers, and cavitation can occur during the computation period. Isotherms are constructed by averaging pressure P over the molecular dynamics trajectory portion up to the beginning of the phase transition ($0 < t < \tau$). Because the selection of the extrapolation function is uncertain (we used polynomials of degrees $n = 2$–4), spinodal points are determined with a certain ambiguity, to within ∼7% for P and ∼3% for ρ. Figure 3 shows that the stability loss in calculations at lower temperatures occurs before $(\mathrm{d}P/\mathrm{d}\rho)_T$ becomes equal to zero. The stability loss and $(\mathrm{d}P/\mathrm{d}\rho)_T = 0$ points approach each other as the temperature increases.

The position of the spinodals of liquid lead and lithium can be preliminarily estimated on the basis of MD calculations of the spinodal of the Lennard-Jones fluid [11, 37] using the concept of thermodynamic similarity with respect to the critical point parameters (figures 3(a) and 4(a)). We performed preliminary estimates of negative pressures corresponding to strongly stretched metastable melts in the temperature range studied. Calculated values are somewhat larger than those obtained in preliminary spinodal estimates by similarity relations (comparison should take into account possible errors in the experimental critical point parameters). The closeness of the calculation results and preliminary spinodal estimates to each other may be considered as the evidence of the universal similarity of the spinodals of simple liquids at low temperatures. This question was deliberately considered in [11, 38]. Note in addition that, as distinct from the results for a Lennard-Jones system [37, 39], the Pb and Li melt spinodals

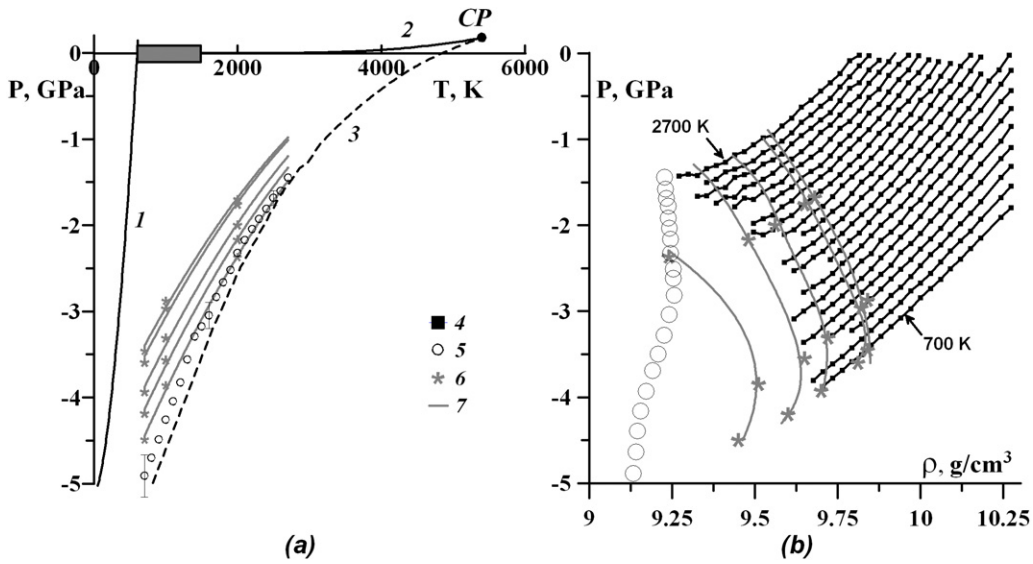

Figure 3. P–T–ρ diagram of lead. *Common to (a) and (b)*: 5 labels the points at which $(\mathrm{d}P/\mathrm{d}\rho)_T = 0$ for the approximation of lead isotherms by polynomials (see figure 1(b)), 6 corresponds to the points at 700, 1000 and 2000 K at which the cavitation rate is 5×10^{27}, 10^{28}, 10^{29}, 3×10^{29} and 10^{30} cm^{-3} s^{-1} (the closer the point is to the spinodal the higher is the corresponding cavitation rate), and curves 7 show estimated points at which the cavitation rate has the above specified values in the temperature range 700–2700 K. (a) (1) Experimental melting curve and its extrapolation to negative pressures by the Simon equation $P/P^* = (T/T_\mathrm{m})^C$–1 ($P^* = 5.11$ GPa, $T_\mathrm{m} = 600$ K, and $c = 1.65$), (2) vaporization curve and (3) liquid lead spinodal estimated by the renormalization of the Lennard-Jones system spinodal with the use of critical point parameters ($T_\mathrm{C} = 5400$ K and $P_\mathrm{C} = 0.175$ GPa [40]); the hatched region corresponds to the supposed coolant working parameters in FIHIF reactors [20, 21]. (b) Isotherms of liquid lead over the temperature range 700–2700 K drawn in steps of 100 K; points 4 obtained in molecular dynamics calculations are linked by solid lines for clarity (also see [14, 15]).

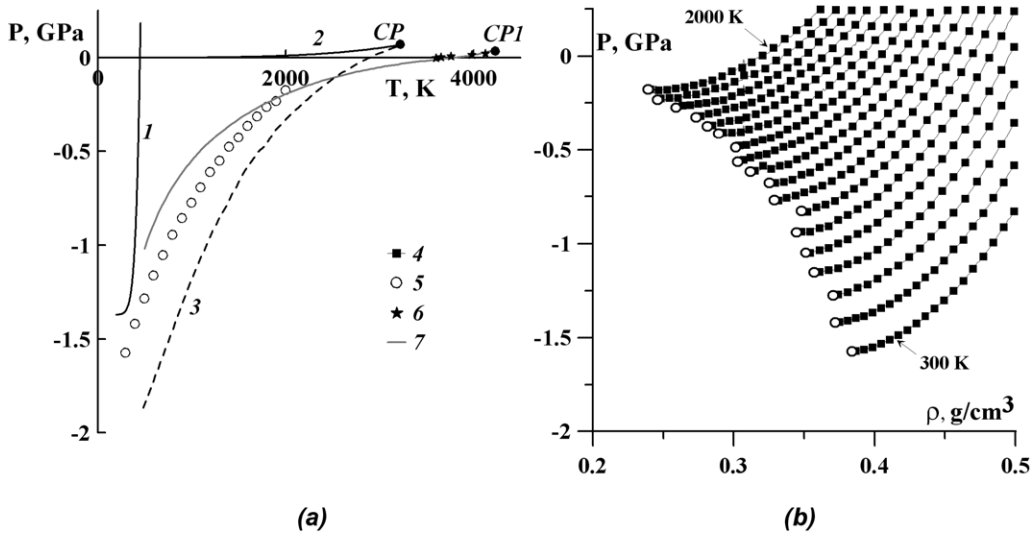

Figure 4. P–T–ρ diagram of lithium. *Common to (a) and (b)*: 5 labels the points at which $(\mathrm{d}P/\mathrm{d}\rho)_T = 0$ for the approximation of lithium isotherms by polynomials (see figure 1(b)), points 6 correspond to the experimental data for the liquid lithium spinodal [55] and 7 is the Furth equation $P_\mathrm{Sp} = P_\mathrm{Vap} - C\sigma^{3/2}(kT)^{-1/2}$ based approximation of experimental points 6, where C is used as a variable. (a) (1) The experimental melting curve and its extrapolation to negative pressures by the Simon equation $P/P^* = (T/T_\mathrm{m})^C - 1$ ($P^* = 1.37$ GPa, $T_\mathrm{m} = 453$ K and $c = 10.13$), (2) the vaporization curve and (3) the liquid lithium spinodal estimated by the renormalization of the Lennard-Jones system spinodal with the use of critical point parameters ($T_\mathrm{C} = 3223$ K and $P_\mathrm{C} = 0.068$ GPa [42]). (b) Isotherms of liquid lithium over the temperature range 300–2000 K drawn in steps of 100 K; points 4 obtained in molecular dynamics calculations are linked by solid lines for clarity.

do not intersect the continuation of the line of lead melting into the region of negative pressures according to the Simon equation, which may be evidence that the crystal and the liquid can be at equilibrium over a wide range of metastable states.

3.3. Kinetic properties of cavitation

The lifetime of a uniform metastable liquid phase along one molecular dynamics trajectory changes in the case of varying of the initial configuration and distribution of particle velocities

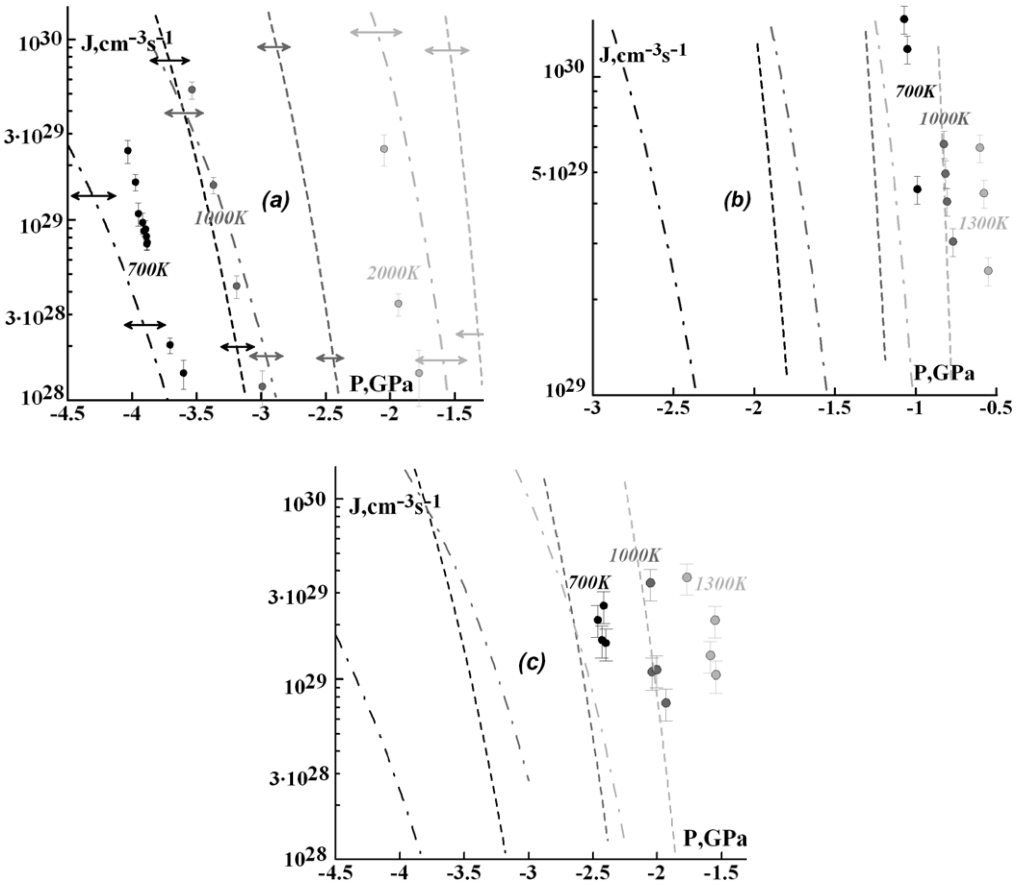

Figure 5. The dependences of cavitation rate on pressure for different melts. MD results are shown by filled circles for the three different values of temperatures using different colors; approaches (8) and (9) are shown by dashed and dot-dashed lines respectively and are colored in the same way. MD results are given with errors due to the error in average lifetime determination. (a) Lead for temperatures 700, 1000 and 2000 K; approaches (8) and (9) are given with errors (arrows) corresponding to the error in experimental value of surface tension [43]. (b) Lithium for temperatures 700, 1000 and 1300 K. (c) $Pb_{83}Li_{17}$ eutectics for temperatures 700, 1000 and 1300 K. Surface tension data for Li and $Pb_{83}Li_{17}$ are taken from [44].

and, initial conditions being equal, integration step [10, 13, 32]. Statistical averaging for the given thermodynamic state (ρ, T, P) is performed over an ensemble of M independent initial configurations, each characterized by the corresponding lifetime τ_i ($i = 1, \ldots, M$). According to the model that treats homogeneous nucleation as a random Poisson process, the distribution of lifetimes τ_i over the ensemble of initial configurations is

$$m(\tau) = \frac{M \cdot \Delta\tau}{\bar{\tau}} \exp\left(-\frac{\tau}{\bar{\tau}}\right), \qquad \bar{\tau} = \frac{1}{M}\sum_{i=1}^{M} \tau_i \quad (7)$$

where $m(\tau)$ is the number of trajectories from the ensemble of M trajectories along which cavitation occurs during the $(\tau, \tau + \Delta\tau)$ time interval. Examples of distributions obtained in our calculations are shown in figure 6(b). We see that model (7) describes fairly well the cavitation process under consideration. To obtain of distributions with a well defined exponential form requires the accumulation of the large statistics ($M > 100$–200). The root-mean-square error determined from M measurements is $\sigma_{\bar{\tau}} = \bar{\tau}/\sqrt{M}$ for the exponential distribution law. The rate of a spontaneous phase transition is usually characterized by the mean number of critical nuclei formed in unit volume per unit time, that is, by the cavitation rate J. The cavitation rate is calculated as $J = 1/(\bar{\tau}V)$. The results are shown in figure 5.

3.4. Concept of spinodal. Elucidation of stability criteria

The above used concepts of spinodal and stability limit need to be considered more deliberately as long as the lifetime of metastable liquid system depends on the system size. It is natural that in a system of a bigger scale a fluctuation of a certain size occurs more easily than in a smaller one. Though the cavitation rate is supposed not to depend on the system volume (as it is normalized by V by definition), there are some questions even in this case: if we calculate the J–P dependence for a certain temperature in the system of volume V_1 and want to obtain a lifetime τ_2 at pressure of the same order of a system of volume $V_2 = 1000V_1$, the time we obtain will be 1000 times shorter than the time τ_1 for V_1. Nothing much it could seem, but since τ_1 is measured in picoseconds in MD τ_2 would have an extremely small value that is not going to come into being at all.

What we could conclude is the fact that the stability limit itself needs to be talked about only with respect to the size of

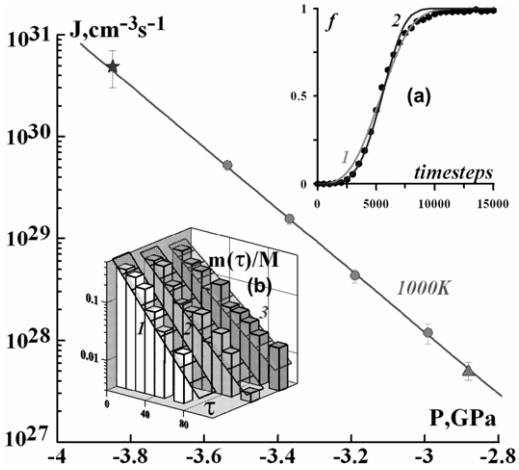

Figure 6. Demonstration of the self-consistency of MD results for two approaches and different numbers of particles in the calculation box. On the main plot is given the dependence of cavitation rate on pressure for $T = 1000$ K: the point obtained from the KJMA (10) approach (star), points obtained from the approach based on distributions for the 13 500 atom system (solid circles) and the 500 000 atom system (triangle). An exponential fit (straight line) of MD data is also given. The insets explain the approaches. *Upper inset* (a) KJMA based cavitation rate estimation approach: the dependence of instantaneous void volume to final void volume ratio on time (timestep = 1.43 fs). MD points are fitted using the KJMA equation: curve 1 for $n = 3$; curve 2 for $n = 4$. The last fit provided the cavitation rate value data point shown by the star on the main plot. *Lower inset* (b) Distribution based cavitation rate estimation approach: number of molecular dynamics trajectories m (τ) from the ensemble of M independent trajectories for which the moment of the beginning of cavitation (lifetime τ_i) lies in the interval $(\tau, \tau + \Delta\tau; \Delta\tau = 15$ ps). Calculation results for various pressure p values at $T = 700$ K are shown: (1) $P = -3.95$ GPa, $M = 46$; (2) $p = -3.91$ GPa, $M = 232$; (3) $p = -3.89$ GPa, $M = 142$. For comparison, the dependences obtained for the model according to which cavitation is a random Poisson process (7) are shown by straight lines (planes). The average lifetime for each distribution/ensemble gives the cavitation rate value.

the system under consideration. In the model calculation we can come very close to the thermodynamic stability limit (or spinodal) determined by the $(\mathrm{d}P/\mathrm{d}\rho)_T = 0$ point, but this condition still is not satisfied. The bigger the size and the number of particles in the calculation cell, the lower the value for the maximal negative pressure it is possible to access in simulation. What is to be noted also is the fact that if even for our model calculations the $(\mathrm{d}P/\mathrm{d}\rho)_T = 0$ point is commonly unreachable, it will not ever be reached in practice seemingly.

3.5. Analysis of pressure and temperature dependence of J

It is interesting to compare the calculation results with the classic nucleation theory predictions. The temperature dependence of the rate of nucleation determined according to Doering–Volmer (see [3, 41]) is

$$J = \frac{\rho}{m}\sqrt{\frac{2\sigma}{\pi m}}\exp\left(-\frac{W}{k_\mathrm{B}T}\right), \qquad W = \frac{16\pi\sigma^3}{3(P-P')^2} \quad (8)$$

where σ is the surface tension along the vaporization line at the temperature T, W is the work of critical nucleus formation and P' is the vapor pressure inside the critical nucleus. Approximation (8) is selected because of the simplicity of the pre-exponential factor, which only contains σ of all the special metastable liquid parameters. The simplified Doering–Volmer approach is

$$J = B\exp\left(-\frac{W}{k_\mathrm{B}T}\right), \qquad W = \frac{16\pi\sigma^3}{3(P-P')^2}. \quad (9)$$

Here B stands for a constant that could be estimated as $B \sim 10^{10}$ s^{-1}. We compare (8) and (9) with the results of molecular dynamics calculations on the assumption that the pressure in the system containing a critical nucleus is equal to the mean pressure along the metastable region ($0 < t < \tau$) and the vapor pressure in the critical bubble is negligibly low, $P' \ll P$. The latter assumption is used because the density of vapor at low temperatures ($T < 0.5T_\mathrm{C}$) is low and critical bubbles were virtually empty. Bubble growth corresponds to the transfer of holes (vacancies) from the liquid rather than the transfer of molecules into the vapor phase. We used the experimental data on the surface tension of melts along the vaporization line [43, 44]. The surface tension σ strongly influences the work of critical nucleus formation and, therefore, the temperature and pressure dependences of the nucleation rate. For this reason, the spread of experimental data is included in the form of the confidence interval $\sigma_\mathrm{min} < \sigma < \sigma_\mathrm{max}$ heuristically constructed on the basis of the uncertainty of the linear approximation of experimental data in the region of high temperatures [14, 15]. Equations (8) and (9) were therefore used to obtain the $\{J(P;\sigma),\ \sigma_\mathrm{min} < \sigma < \sigma_\mathrm{max}\}$ regions that correspond to the classic nucleation theory approach data.

It follows from figure 5 that the classic nucleation theory results are not in quantitative agreement with MD results and do not even qualitatively reproduce them correctly. Actually, there is no general way in which approaches (8) and (9) differ from MD results. The discrepancy between theory and calculation results cannot be completely eliminated by including the dependence of surface tension on surface curvature (e.g., see [3, 45, 46]). It follows from the existence of both lower and upper positions of the two approaches (8) and (9) with respect to MD data. The calculation results may be considered as evidence of the fact that the surface tension of bubbles of critical size is larger than its value for a plane interface or the work of critical nucleus formation is underestimated for Pb (see figure 5(a)) and overestimated for Li and $Pb_{83}Li_{17}$ (see figures 5(b) and (c)). Note that the consistent comparison of molecular dynamics simulation results and various classic nucleation theory approximations should involve the determination of the temperature dependence of surface tension along the liquid–vapor equilibrium line performed using the same molecular dynamics model. One of the possible reasons why the classic nucleation theory approximations are not in acceptable agreement with the calculation results is the critical nucleus size estimated according to the theory (for Pb melt). It is $N_n = (\rho/m)(4\pi/3)(2\sigma/|P|)^3 \approx 1$ atom ($\rho/m = 2.82 \times 10^{28}$ m^{-3}, $T = 700$ K, $\sigma = 0.431$ N m^{-1}, $P = -3.89$ GPa), which is, generally, outside the applicability range of the

macroscopic classic nucleation theory approach in the region under consideration.

The homogeneous nucleation rate exponentially decreases far from the stability limits of the metastable liquid because of the high activation barrier of spontaneous fluctuation cavity formation. Cavitation in the coolant in the practically important region of power plant functioning parameters could probably occur by the heterogeneous mechanism of nucleation on impurities and inhomogeneities (such as, for instance, lithium atom clusters in the $Pb_{83}Li_{17}$ eutectic [20, 21]). MD heterogeneous cavitation rate calculations can be performed using a correct model of interactions with impurity atoms.

3.6. Self-consistency of the results for different volumes. Multi-bubbling

Since the discussed method of calculations can be used at various numbers of particles, the question arises of the extent to which the results depend on the size of the calculation cell. We obtained the dependences of the pressure and the temperature in the metastable liquid on the number of particles at the computationally reachable values (from 500 to 500 000 particles in the cell). It is found that the size of the system substantially influences the fluctuations of the parameters with respect to their mean values rather than the mean values themselves. This fact is in accordance with theoretical predictions. The cavitation rate is independent of volume because the number of critical nuclei increases as the volume grows.

There is, actually, another way to estimate the value of cavitation rate from only one calculation of a large-scale system. It is based on the Kolmogorov–Johnson–Mehl–Avrami (KJMA) equation describing the time dependence of the fraction transformed during the phase transition [47–49]:

$$f = 1 - \exp\left(-kt^n\right). \tag{10}$$

For spontaneous nucleation $n = 4$ and $k = J\upsilon^3\pi/3$, for site-saturated nucleation $n = 3$ and $k = 4N\upsilon^3\pi/3$, where J is the nucleation rate, N is the initial site concentration and υ is the new phase cluster (e.g. bubble, drop) growth rate. Using this equation and having the MD trajectory for a large-scale system of about 1 million atoms where there are enough bubbles (about 50–100), it is possible to make estimations of the cavitation rate from only one calculation. The MD results compared with the Kolmogorov–Avrami equation are shown in figure 6(a). It is seen from the figure that in the initial stage MD results are better fitted with the approach (10) with $n = 4$, and in the final stage MD results correspond to (10) with $n = 3$. This seems natural because initially there were no nucleation sites; they appeared in the course of time.

KJMA equation based cavitation rate estimation shows approximately the same value as for the method of simulation of the ensemble of the MD runs for smaller number of particles (figure 6). The number of atoms does not affect the dependence of cavitation rate on pressure: in figure 6 are shown the results for the distribution based approach for 13 500 atom and 500 000 atom containing systems that are lying on a straight line exactly. The case of multi-bubbling and the dynamics of the decay were also considered in [15].

3.7. Cavitation in Pb–Li

When we have two different types of atoms in the simulation the potential energy calculation is not different at all except that the summation over atom type is included. The formula for the potential energy of a particle is

$$U_i = \sum_{i<j} \phi_{\alpha\beta}(r_{ij}) + F_\alpha\left(\sum_{i\neq j}\rho_\alpha(r_{ij})\right) \tag{11}$$

where F is the embedding energy, which is a function of the atomic electron density ρ, ϕ is a pair potential interaction, and α and β are the element types of atoms i and j respectively. The multi-body nature of the EAM potential is a result of the embedding energy term. Both summations in the formula are over all neighbors j of atom i within the cutoff distance. Let us consider a Pb atom, for example, that is, $\alpha =$ Pb. Effective electron density on it is induced by both Li and Pb type atoms within a cutoff sphere: $\rho_\alpha = \rho_{\mathrm{Pb}}$ in the sum in the brackets. As the embedding function we take the one for Pb: $F_\alpha = F_{\mathrm{Pb}}$. Pair interactions are calculated absolutely the same way as for the single-atom type case. The only unknown parameter here is the cross-Pb–Li pair interaction function: $\phi_{\alpha\beta} = \phi_{\mathrm{Pb}}$ if $\beta =$ Pb; $\phi_{\alpha\beta} = \phi_{\mathrm{PbLi}}$ if $\beta =$ Li.

We use single-atom potentials for Pb and Li to construct a cross-Pb–Li interaction potential. Based on the approach from [50] we modified functions from (11):

$$\rho(R) \to C\rho(R) \qquad F(\rho) \to F(\rho/C). \tag{12}$$

This transformation does not change the Hamiltonian itself but provides us with an opportunity to vary the cross-Pb–Li pair interaction function by changing constants C for each atom type:

$$\phi_{\mathrm{PbLi}}(r) = \frac{1}{2}\left(\frac{\rho_{\mathrm{Pb}}}{\rho_{\mathrm{Li}}}\phi_{\mathrm{Li}}(r) + \frac{\rho_{\mathrm{Li}}}{\rho_{\mathrm{Pb}}}\phi_{\mathrm{Pb}}(r)\right). \tag{13}$$

Thus, having chosen particular constants for each metal, we can calculate the pair correlation function $g(r)$ from MD and then according to the formula

$$a(K) = 1 + n_0\int_0^\infty \left[g(r) - 1\right]\frac{\sin(Kr)}{Kr}r^2\,\mathrm{d}r \tag{14}$$

we can calculate static structure factor $a(K)$ as a functional depending on C_{Li} and C_{Pb}. Finally, having experimental data on $a(K)$ from [51] we can calculate mean square deviation. Such an algorithm was applied to the constant interval of {0.1–10} and it was shown that the best correspondence is reached at the values of constants $C_{\mathrm{Li}} = 0.7$, $C_{\mathrm{Pb}} = 0.9$.

The results on the dependence of cavitation rate on pressure for $Pb_{83}Li_{17}$ (see figure 5(c)) were obtained using the cross-Pb–Li interaction potential described above. Compared with the results for pure Pb and Li, the results for $Pb_{83}Li_{17}$ tell us that there is probably the same mechanism of bubble formation in a two-component system as for a one-component system under the conditions studied. This can be assumed from the same steepness of the J–p curve for PbLi as for the pure metals.

Having obtained the cross potential for Pb–Li interactions we started the study of the heterogeneous cavitation on

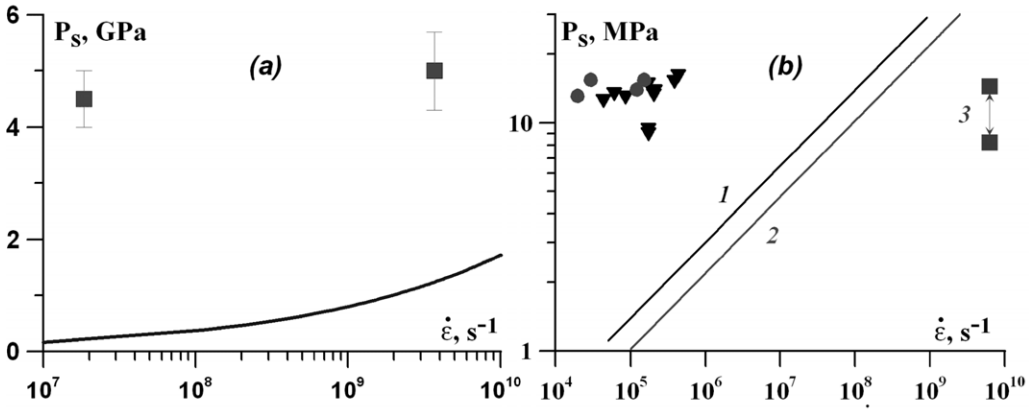

Figure 7. Comparison of spall strength P_S according to the Grady criterion [52] with MD and experimental data: (a) MD data on P_S for Pb (squares) compared with (15); (b) experimental data from [53, 54] on P_S for hexane (circles) and ethanol (triangles) compared with approach (15)—lines 1, ethanol; 2, hexane; 3, estimation of P_S results for both substances by renormalizing of MD calculation of Lennard-Jones system, critical point parameters being known [11, 39].

impurities. The bubble formation in this case occurs on the interface between two atomic types. Impurities are formed by lithium atom clusters inside the media of lead atoms. Preliminary results showed a strong dependence of the maximum reachable value of negative pressure on the heterogeneity. Thus, while $P_{\max}$ for Pb is in the interval of 4.5–5.0 GPa, for a Pb–Li heterogeneous system this value is about 2–2.5 GPa according to our preliminary calculations.

4. Spallation criteria

While calculating the equation of state for liquid metals we obtained some data on the adiabatic expansion of metals under consideration, especially on the spall strength. Here it seems reasonable to consider the spallation results of our MD in comparison with hydrodynamical spallation criterion of Grady [52]. According to this criterion, the spall strength of matter could be estimated using several of its properties:

$$P_S = (6\rho^2 c^3 \sigma \dot{\varepsilon})^{1/3} \tag{15}$$

where ρ stands for density, c is the sound velocity, σ is the surface tension and $\dot{\varepsilon} = \frac{1}{V}\frac{\mathrm{d}V}{\mathrm{d}t}$ is the expansion rate. Both MD calculations (for Pb) and experimental results (for ethanol, hexane and water from [53, 54]) have only qualitative agreement compared with this criterion. The value of P_S produced by (15) is significantly smaller than it appears to be in MD simulation (see figure 7). Experimental parameters of Pb are taken from [43].

5. Conclusions

An approach has been developed for MD modeling and simulation of cavitation in metastable liquids. It includes the following:

- calculation of the equation of state at negative pressures;
- treatment of homogeneous cavitation rate;
- elucidation of the concept of the limit of stability (spinodal).

The examples for liquid metal EAM models of Pb, Li and $Pb_{83}Li_{17}$ have been given:

- the self-consistency of MD results for small and large systems is shown and both approaches (single-bubble and multi-bubble cavitation) provide the same data on cavitation kinetics,
- the theoretical approaches based on classical nucleation theory fail to describe MD results,
- the cross-Pb–Li interaction potential is constructed and
- it is shown that most probably cavitation in $Pb_{83}Li_{17}$ has the same origin as for Pb and Li.

The importance of study of cavitation as a stochastic phenomenon has been shown. The approach uses stochastic features of the MD method in explicit form and is based on a physically proven choice of the ensemble of initial nonequilibrium states for averaging the relaxation MD runs [56].

Cavitation in metastable melts at both negative pressures and stationary stretching rates is treated. The examples of Grady spallation criteria failing to describe MD and experimental data are shown. Stability limits for liquid Pb, Li and $Pb_{83}Li_{17}$ are estimated in a wide range of pressures and temperatures significantly lower than critical temperatures ($T < 0.5Tc$). Elucidation of stability criteria is proposed. Cavitation kinetics and dynamics are studied for different temperatures. It is shown that theoretical approaches based on the classical theory of nucleation and the MD results provide different estimations of cavitation rate.

It is shown that using the KJMA equation for the bubble growth kinetics it is possible to estimate the value of cavitation rate from only one calculation of a rather large (million-atomic) 'multi-bubbling' system. This estimate appears to be of the same order as for the above described method of simulation of the MD run ensemble for smaller systems or the distribution based method. In fact, the latter approach provides a more accurate value of cavitation rate. Thus it can be concluded that in the case of homogeneous cavitation it is crucial to calculate a large-scale system only to study states of matter

rather far from stability limit. Since cavitation rate is defined as $J = 1/(\bar{\tau} V)$, the bigger the system volume for the same value of lifetime/calculation time the lower is the cavitation rate value and respectively the farther we go from the stability limit.

The approach has a universal nucleation character. It is applied as well to the following:

- nucleation in solids at both constant superheating and stationary superheating rate [10];
- cavitation in single crystals and nanocrystals at both negative pressures and stationary stretching rates [11, 57, 56].

The approach can be applied to solidification and vitrification too.

The examples of challenging problems that can be considered using the described method include the following:

- heterogeneous nucleation and cavitation (a physically proven choice of the ensemble of initial nonequilibrium states is not clear);
- extension of the approach outside temporal and space scales accessible for the MD method;
- second stage of cavitation (bubble collapse) study and incorporation of MD results in continuum media mechanics.

Acknowledgments

We are grateful to V G Baidakov and S P Protsenko, V E Fortov and S A Medin for discussions and interest in our work. The calculations are partly performed on the computer cluster of FMBF of the Moscow Institute of Physics and Technology. TB and VS are grateful to the Dinastiya Foundation for Nonprofit Programs for support. This study was supported by the following: the programs of fundamental research of the Russian Academy of Sciences 'Extreme state of matter research' and 'Fundamental problems of computer science' and section program 'Phase state stability and critical regimes of heat and mass transfer'; The Russian Ministry of Education and Science project RNP 2.1.1.712 'Computer simulation of metals in the region of phase transitions and under extreme conditions'; The Russian Foundation for Basic Research grant 05-08-65423.

References

[1] Volmer M 1939 *Kinetik der Phasenbildung* (Dresden: Theodor. Steinkopff Verlag)
[2] Frenkel J 1946 *Kinetic Theory of Liquids* (London: Oxford University Press)
[3] Skripov V P 1974 *Metastable Liquids* (New York: Wiley)
[4] Skripov V P and Faizullin M Z 2003 *Crystal–Liquid–Vapor Phase Transitions and Thermodynamic Similarity* (Moscow: Fizmatlit) (in Russian)
[5] Skripov V P and Koverda V P 1984 *Spontaneous Crystallization of Supercooled Liquids* (Moscow: Nauka) (in Russian)
[6] Novikov I I 2000 *Termodynamics of Spinodals and Phase Transitions* (Moscow: Nauka) (in Russian)
[7] Debenedetti P G 1998 *Metastable Liquids: Concepts and Principles* (Princeton: Princeton University Press)
[8] Kinjo T and Matsumoto M 1998 *Fluid Phase Equilib.* **144** 343
[9] Norman G E and Stegailov V V 2002 *Dokl. Akad. Nauk* **386** 328
Norman G E and Stegailov V V 2002 *Dokl. Phys.* **47** 667 (Engl. Transl.)
[10] Norman G E and Stegailov V V 2004 *Mol. Simul.* **30** 397
[11] Kuksin A Yu, Norman G E and Stegailov V V 2007 *Teplofiz. Vys. Temp.* **45** 43
Kuksin A Yu, Norman G E and Stegailov V V 2007 *High Temp.* **45** 37 (Engl. Transl.)
[12] Baidakov V G and Protsenko S P 2003 *Teplofiz. Vys. Temp.* **41** 231
Baidakov V G and Protsenko S P 2003 *High Temp.* **41** 195 (Engl. Transl.)
[13] Baidakov V G and Protsenko S P 2004 *Dokl. Akad. Nauk* **394** 752
Baidakov V G and Protsenko S P 2004 *Dokl. Phys.* **49** 69 (Engl. Transl.)
[14] Bazhirov T T, Norman G E and Stegailov V V 2005 *Dokl. Akad. Nauk* **405** 325
Bazhirov T T, Norman G E and Stegailov V V 2005 *Dokl. Phys.* **50** 570 (Engl. Transl.)
[15] Bazhirov T T, Norman G E and Stegailov V V 2006 *Russ. J. Phys. Chem.* **80** S90
[16] Bazhirov T T, Norman G E and Stegailov V V 2007 *Comput. Phys. Commun.* **177** 41
[17] Matsumoto M, Miyamoto K, Ohguchi K and Kinjo T 2000 *Progr. Theor. Phys. Suppl.* **138** 728–9
[18] Galimov E *et al* 2004 *Dokl. Akad. Nauk* **395** 187
Galimov E *et al* 2004 *Dokl. Phys.* **49** 150 (Engl. Transl.)
[19] Taleyarkhan R, West C, Cho J S, Lahey R T Jr, Nigmatulin R I and Block R 2002 *Science* **295** 1868
[20] Medin S A, Orlov Yu N, Parshikov A N and Suslin V M 2004 *Preprint No. 41*IPM im. M. V. Keldysha RAN (Keldysh Institute of Applied Mathematics, Rus. Acad. Sci., Moscow) (in Russian)
[21] Medin S *et al* 2005 *Nucl. Instrum. Methods Phys. Res.* **544** 300
[22] Basko M M *et al* 2005 Inertial confinement nuclear synthesis *Modern State and Energetic Perspectives* ed B Yu Sharkov (Moscow: Fizmatlit) (in Russian)
[23] Hassanein A 2000 *Laser Part. Beams* **18** 611
[24] Hassanein A and Konkashbaev I 2001 *Argonne National Laboratory Report ANL-ET/01-13*
[25] Vinogradov V E and Pavlov P A 2002 *J. Eng. Thermophys.* **11** 353
[26] Daw M S and Baskes M I 1984 *Phys. Rev.* B **29** 6443
[27] Belashchenko D K 1999 *Usp. Fiz. Nauk* **169** 361
Belashchenko D K 1999 *Phys. Usp.* **42** 297 (Engl. Transl.)
[28] Lim H S, Ong C K and Ercolessi F 1992 *Surf. Sci.* **269** 1109
[29] Li Y, Blaisten-Barojas E and Papaconstantopoulos D A 1998 *Phys. Rev.* B **57** 15519
[30] Srinivasan S G and Baskes M I 2004 *Proc. R. Soc.* A **460** 1649
[31] Bilalbegovic G and Lutz H O 1997 *Chem. Phys. Lett.* **280** 59
[32] Valuev A A, Norman G E and Podlipchuk V Yu 1989 *Mathematical Modeling: Physico-Chemical Properties of Substances* ed A A Samarskii and N N Kalitkin (Moscow: Nauka) p 5 (in Russian)
[33] Robbins M O, Grest G S and Kremer K 1990 *Phys. Rev.* B **42** 5579
[34] Norman G E and Stegailov V V 2002 *Comput. Phys. Commun.* **147** 678–83
[35] Norman G E and Stegailov V V 2001 *Zh. Eksp. Teor. Fiz.* **119** 1011
Norman G E and Stegailov V V 2001 *J. Exp. Theor. Phys.* **92** 879 (Engl. Transl.)
[36] Iosilevskii I L and Chigvintsev A Yu 2003 *Electronic J. Investigated in Russia* http://zhurnal.ape.relarn.ru/artisles/2003/003.pdf (in Russian)

[37] Baidakov V G and Protsenko S P 2005 *Dokl. Akad. Nauk* **402** 754
Baidakov V G and Protsenko S P 2005 *Dokl. Phys.* **50** 303 (Engl. Transl.)
[38] Bazhirov T T, Kuksin A Yu, Norman G E and Stegailov V V 2007 *Zh. Fiz. Khim.* **81** 1165
Bazhirov T T, Kuksin A Yu, Norman G E and Stegailov V V 2007 *Russ. J. Phys. Chem.* A **81** 1016 (Engl. Transl.)
[39] Baidakov V G and Protsenko S P 2005 *Phys. Rev. Lett.* **95** 015701
[40] Ternovoi V Ya, Fortov V E, Kvitov S V and Nikolaev D N 1996 *Shock Compression of Condensed Matter–1995* ed S C Schmidt and W C Tao (New York: AIP) Part 1, p 81
[41] Blander M and Katz J L 1975 *AIChE J.* **21** 833
[42] Fortov V E, Khrapak A G and Yakubov I T 2004 *Physics of Nonideal Plasma* (Moscow: Fizmatlit) (in Russian)
[43] Babichev A P *et al* 1991 *Physical Values: A Handbook* ed I S Grigor'ev and E Z Meilikhov (Moscow: Energatomizdat) (in Russian)
[44] Sze D K, Moir S and Zinkle S 1999 *APEX Interim Report: Data Base for Liquid Breeders and Coolants* (chapter 8)
[45] Schmelzer J W P, Gutzow I and Schmelzer J Jr 1996 *J. Colloid Interface Sci.* **178** 657
[46] Insepov Z and Hassanein A 2005 *J. Nucl. Mater.* **337–339** 912
[47] Kolmogorov A N 1937 *Bull. Acad. Sci. USSR Ser. Math.* **3** 355 (in Russian)
[48] Johnson W A and Mehl R F 1939 *Trans. Metall. Soc. AIME* **135** 416
[49] Avrami M 1939 *J. Chem. Phys.* **7** 1103
[50] Landa A *et al* 2000 *Acta Mater.* **48** 1753
[51] Ruppersberg H and Egger H 1975 *J. Chem. Phys.* **63** 4095
[52] Grady D 1988 *J. Mech. Phys. Solids* **36** 353
[53] Utkin A V, Sosikov V A and Bogach A A 2003 *J. Appl. Mech. Tech. Phys.* **44** 174
[54] Utkin A V, Sosikov V A and Fortov V E 2006 *Shock Compression of Condensed Matter–2005* vol 845, ed M D Furnish, M Elert, T P Russell and C T White (New York: AIP) p 896
[55] Trukhanenok A N, Nikolaev D N and Ternovoi V Ya 2006 *Fizika Ekstremalnykh Sostoyanii Veschestva* ed Fortov V E *et al* p 16 (in Russian)
[56] Kuksin A Y, Morozov I V, Norman G E, Stegailov V V and Valuev I A 2005 *Mol. Simul.* **31** 1005
[57] Kuksin A Yu and Yanilkin A V 2007 *Dokl. Akad. Nauk* **413** 615
Kuksin A Yu and Yanilkin A V 2007 *Dokl. Phys.* **52** 186 (Engl. Transl.)